ACS APPLIED MATERIALS & INTERFACES

Research Article

www.acsami.org

Reduction Mechanisms of Ethylene Carbonate on Si Anodes of Lithium-Ion Batteries: Effects of Degree of Lithiation and Nature of Exposed Surface

Julibeth M. Martinez de la Hoz,[†,‡] Kevin Leung,[§] and Perla B. Balbuena*[,†,‡]

[†]Department of Chemical Engineering and [‡]Department of Materials Science and Engineering, Texas A&M University, College Station, Texas 77843, United States

[§]Sandia National Laboratories, MS 1415, Albuquerque, New Mexico 87185, United States

Supporting Information

ABSTRACT: *Ab initio* molecular dynamics simulations are used to identify mechanisms of reduction of ethylene carbonate on Si surfaces at various degrees of lithiation, where the low-coordinated surface Si atoms are saturated with O, OH, or H functional groups. The lowest Si content surfaces are represented by quasi-amorphous $LiSi_4$ and $LiSi_2$; intermediate lithiation is given by LiSi crystalline facets, and the highest Li content is studied through $Li_{13}Si_4$ surfaces. It is found that ethylene carbonate (EC) reduction mechanisms depend significantly on the degree of lithiation of the surface. On LiSi surfaces EC is reduced according to two different two-electron mechanisms (one simultaneous and one sequential), which are independent of specific surface functionalization or nature of exposed facets. On the less lithiated surfaces, the simultaneous two-electron reduction is found more frequently. In that mechanism, the EC reduction is initiated by the formation of a C−Si bond that allows adsorption of the intact molecule to the surface and is followed by electron transfer and ring-opening. Strongly lithiated $Li_{13}Si_4$ surfaces are found to be highly reactive. Reduction of adsorbed EC molecules occurs via a four-electron mechanism yielding as reduction products CO^{2-} and $O(C_2H_4)O^{2-}$. Direct transfer of two electrons to EC molecules in liquid phase is also possible, resulting in the presence of $O(C_2H_4)OCO^{2-}$ anions in the liquid phase.

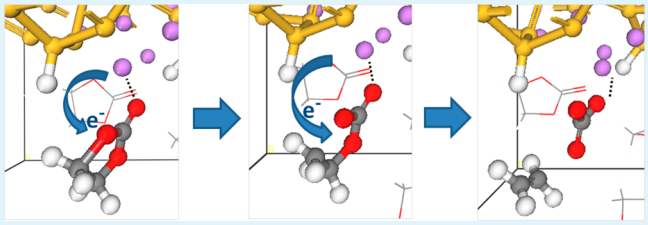

KEYWORDS: *solid electrolyte interphase reaction, ab initio molecular dynamics, solvent reduction, Li-ion batteries*

1. INTRODUCTION

Lithium-ion batteries play an important role providing portable energy to popular electronic devices such as cell phones and laptops. However, the performance of the battery regarding life cycle stability and energy density is still insufficient to satisfy the needs of high-end electronics or electric cars.[1−3] In terms of improving the energy density of the battery, silicon is one of the most promising materials due to its large charge storage capacity, reported to be about 10 times higher than that of graphitic anodes.[4−7] Unfortunately, silicon undergoes significant structural changes during lithium intercalation, which causes mechanical damage and pulverization of the electrode after a few hundred lithiation/delithiation cycles.[4−7] A factor believed to help improve the mechanical stability of the anode is the formation of a passivating layer known as solid electrolyte interphase (SEI).[8,9] The SEI layer is formed on the silicon surface due to reduction of organic solvent and electrolyte components,[10] and its thickness, structure, and chemical composition have been found experimentally to depend on the solvent, electrolyte, additives employed, and structure of the electrode.[4,11,12] Given the importance of the SEI layer stabilizing the anode and hindering further decomposition of the electrolyte, efforts must be focused on the study of the various stages of the process. Of special interest is the reduction of electrolyte species on lithiated silicon surfaces as a function of the degree of lithiation, surface facet exposed, and surface functionalization. Electrolyte components may be in direct contact with the fresh lithiated anode during the first lithium intercalation, and also after cracking of the SEI layer due to expansion/contraction of silicon during lithiation/delithiation cycles.[13] A thorough understanding of the reduction of electrolyte species on the anode surface will help elucidate the factors playing a role in the formation of the SEI layer.

In this work, we investigate the reduction of ethylene carbonate (EC) on lithiated surfaces with different compositions of lithium using *ab initio* molecular dynamics (AIMD) based simulations. The mechanism is described in detail for the LiSi-100 and the LiSi-101 surfaces. Lithium monosilicide (LiSi) is one of the first stable crystalline phases expected during lithiation of silicon at high temperatures.[14] Subsequently, the effect of lower lithium content is analyzed by comparing the EC reduction process on $LiSi_2$-100, $LiSi_4$-100, as well as with the

Received: October 4, 2013
Accepted: November 13, 2013
Published: November 13, 2013

Table 1. Calculated Lattice Constants, Fractional Coordinates, and Volume of the Unit Cell of Bulk LiSi[a]

lattice constants (Å)			Li fractional coordinates			Si fractional coordinates		
a	*c*	vol (Å^3)	*x*	*y*	*z*	*x*	*y*	*z*
9.3607	5.7281	501.9163	0.0802	0.8853	0.0567	0.1103	0.9526	0.5955

[a]The space group is $I4_1/a$.

Table 2. Lattice Constants and Crystallographic Information of the LiSi-100 and LiSi-101 Surfaces Used for the AIMD Simulations[a]

		lattice constants (Å)					
surface	space group	*a*	*b*	*c*	no. Li/no. Si	no. EC (liquid phase)	no. EC (gas phase)
LiSi-100	*P*1 (triclinic)	9.36	11.46	27.2	48/48 (8)	10	1
LiSi-101	*P*1 (triclinic)	21.95	9.36	24.0	64/64 (8)	13	1

[a]The number of Li and Si atoms in each system is also shown with the number of two-fold coordinated silicon atoms in parentheses. Additionally, the number of EC molecules employed to model the liquid and gas phase in each system is shown.

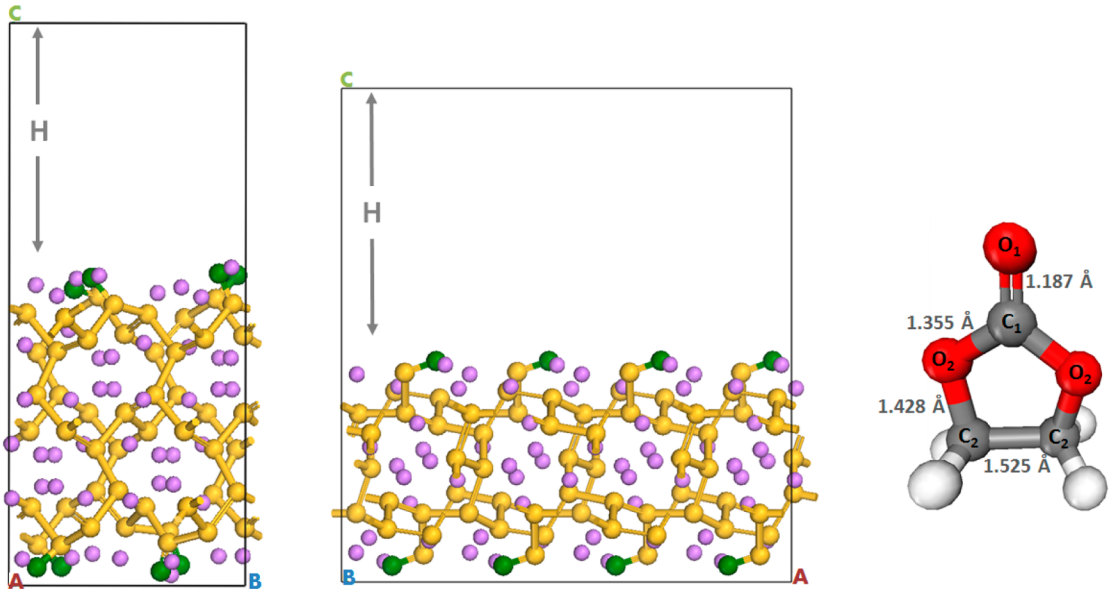

Figure 1. LiSi unit cells and EC molecule utilized in the AIMD simulations. (left) LiSi-100 surface (middle) LiSi-101 surface. The distance *H*, separating the slab from its periodic image in the *z*-direction, corresponds to 10 Å in the 100-surface and 8 Å in the 101. Silicon atoms are yellow; lithium atoms are pink. The green atoms represent the functional groups (−H, −O, and −OH) capping the two-fold coordinated silicon atoms in each surface. (right) Optimized ethylene carbonate molecule (C_2 symmetry). Calculated bond lengths and symmetry are in agreement with previously reported values.[38] Carbon atoms are grey, oxygen atoms are red, and hydrogen atoms are white.

higher lithiation limit, the strongly lithiated $Li_{13}Si_4$ surface. Voltages corresponding to these lithiation stages are >0.39 V vs Li^+/Li metal for $LiSi_2$-100 and $LiSi_4$-100, 0.39 V for LiSi, and about 0.2 V for $Li_{13}Si_4$.[15,16] Surface functionalization is explored through addition of O, H, and OH atoms to low-saturated Si atoms on the surface. The presence of other solvent or additive molecules may affect the reduction because they may reduce at different potentials, and consequently charged intermediate products of one reduction may induce further reductions. For example, some additives such as vinylene carbonate (VC) are known to be reduced earlier than EC,[17] but EC reduces before the linear carbonates such as diethyl carbonate (DEC) or dimethyl carbonate (DMC).[18] Comparisons between propylene carbonate (PC) and EC were also addressed in previous work where we examined electron transfer to solvated Li ions.[19] We note that when a solvated Li ion complex is close to the negative electrode, the complex may receive an electron from the surface and depending on the cell potential that electron may reduce either the Li ion or the EC molecule. On Si anodes, at potentials higher than 0.39 V (vs Li/Li^+), only solvent molecules will be reduced. This is one of the cases we are addressing in this work, on surfaces with very low Li concentrations. At lower cell potentials, a surface electron may reduce the solvated Li ion, triggering a desolvation process. Consequently, some solvent molecules become free and able to be reduced by the surface; this is another case we are addressing in this work. Finally, also at low potentials where the Li ion may be reduced, there is a significant amount of solvent molecules that are not in the first solvation shell of the ion. Those molecules have high mobilities and can get close to the surface and become reduced by various mechanisms described in this work. Thus, while in our earlier reports we focused on reduction of solvated species, in this paper, we concentrate on surface effects, specifically on the Si anode under various states of lithiation. These results provide a first step to develop a better understanding of the SEI layer formation, and they are expected to help develop new strategies to mitigate silicon-anode degradation in Li-ion batteries.

2. COMPUTATIONAL AND SYSTEM DETAILS

2.1. Reduction of Ethylene Carbonate (EC) on Lithium Monosilicide (LiSi). To study the reduction of EC on lithium monosilicide surfaces, a bulk $Li_{16}Si_{16}$ system was optimized using density functional theory (DFT). The structure of LiSi consists of three-fold coordinated Si^- anions forming a series of eight-membered rings linked together, and Li^+ cations within the cavities of the three-dimensional network formed by the rings.[20,21] The calculated lattice constants (a and c), fractional coordinates of Li and Si atoms, and volume of the unit cell are shown in Table 1. Comparisons with experimental and other theoretical studies show good agreement of our calculation with reported parameters.[21−23] Subsequently, the optimized bulk was cleaved to generate five different low-index surfaces corresponding to the (001), (100), (101), (110), and (111) crystallographic planes. Surface energies were calculated through DFT calculations using eq 1,[24] where σ is the surface energy, A is the total area of the surface in the slab model, E_{slab} is the total energy of the slab model for the surface, E_{bulk} is the energy of the bulk material, and n is the number of formula units of the bulk in the slab model:

$$\sigma = \frac{1}{A}[E_{slab} - nE_{bulk}] \quad (1)$$

Calculated surface energies correspond to 0.059, 0.039, 0.049, 0.054, and 0.055 eV/Å^2 for the (001), (100), (101), (110), and (111) surfaces, respectively. The surface with the lowest energy is the (100) followed by the (101); consequently, these two surfaces were chosen to analyze the reduction of EC on lithium monosilicide. However, in order to eliminate dangling bonds on the systems, two-fold coordinated silicon atoms on the surfaces were terminated using one −H, −O, or −OH functional group. These functionalized LiSi surfaces were then optimized and the reduction of EC molecules was studied in the six different resulting systems (LiSi-100-H, LiSi-100-O, LiSi-100-OH, LiSi-101-H, LiSi-101-O, and LiSi-101-OH), using AIMD simulations. Previous reports have shown the capabilities of AIMD to model liquid EC decomposition on different electrode materials within accessible time scales.[25−28] Crystallographic information on the unit cells modeling the LiSi-100 and the LiSi-101 surfaces, along with the number of EC molecules employed to model the liquid and the gas phases, are reported in Table 2. The systems are depicted in Figure 1, together with an optimized EC molecule.

Optimizations were performed using the Vienna ab initio simulation package VASP,[29−33] with the Perdew−Burke−Ernzerhof functional (GGA-PBE)[34] and the projector augmented wave (PAW) pseudopotentials provided in the VASP databases describing electron−ion interactions.[35,36] The plane wave was expanded up to a cutoff energy of 400 eV. The convergence criteria for ionic relaxation loop and for electronic self-consistent iteration were set to 10^{-3} and 10^{-4} eV respectively. A Gaussian smearing with a width of 0.05 eV was employed, and a 4 × 4 × 1 k-points Monkhorst−Pack[37] mesh sampling was used in the surface Brillouin zone.

The AIMD simulations were carried out on the optimized LiSi surfaces in contact with liquid-phase EC (density = 1.32 g/cm^3) and also gas-phase EC (density ≈ 0.1 g/cm^3), using the *NVT* ensemble at 400 K and a time step of 1 fs. The Nose thermostat was used to control the temperature oscillations during the simulation with a Nose-mass parameter of 0.5, which gives a frequency of oscillation corresponding to 176 time steps. A Γ-point Brillouin zone sampling was applied in this case with a planewave energy cutoff of 300 eV. Increasing the cutoff energy to 400 eV yielded similar qualitative results but decreased the number of EC molecules adsorbing on the given surface. Given that the aim of this work is to study the EC-adsorption mechanism, the cutoff energy chosen was that allowing a slightly larger number of molecules reducing on each surface (300 eV) but following the same mechanism as with the larger cutoff (400 eV). In every case, EC molecules were placed randomly in the liquid phase and a molecular dynamics minimization was performed using the consistent valence force field (CVFF) as implemented in the DISCOVER simulation software.[39] CVFF is considered good for modeling small organic crystals and gas phase structures.[40] For the minimization, a smart algorithm was used combining steepest descent, conjugate gradient, and Newton methods. The maximum force among all the atoms in the system required for convergence was set to 0.001 kcal mol^{-1} Å^{-1}. Subsequently, the minimized system was allowed to *relax* during the first 2 ps of AIMD simulation with an imposed charge of +4|e| to avoid reduction of the EC molecule. After this *relaxation* time, all the systems were allowed to run for additional 8 ps. Two different initial configurations were used for each of the surfaces studied. Bader charge analysis was used to perform charge calculations.[41,42] Within this method, the total electronic charge of an atom is approximated by the charge enclosed within the Bader volume defined by zero flux surfaces.

2.2. Reduction of Ethylene Carbonate (EC) on $LiSi_2$-100 and $LiSi_4$-100 Surfaces. In order to evaluate the effect of lower lithium content in the silicon surface, the EC reduction process was also studied on $LiSi_2$-100 and $LiSi_4$-100 surfaces. The slabs were formed by randomly removing lithium ions from the LiSi-100 surface and re-optimizing the surface with lower lithium content using DFT. Two-fold coordinated silicon atoms were then terminated using one hydrogen atom with the purpose of eliminating dangling bonds. These systems were subsequently employed to perform AIMD simulations interacting with liquid EC at 400 K. Parameters employed for DFT and AIMD simulations are the same reported in the previous section.

2.3. Reduction of Ethylene Carbonate (EC) on $Li_{13}Si_4$-010 Surface. The high-lithiation limit was evaluated by studying the reduction of EC on the $Li_{13}Si_4$ surface, which is a disordered alloy found on cycled materials and made up of silicon dumbbells and isolated silicon atoms as described by Chevrier et al.[22] The 010 crystallographic plane was chosen to model the surface since it represents one of the most stable planes for this stoichiometry.[28] In this case, no silicon atoms are on the topmost layers of the surface; therefore elimination of dangling bonds was not necessary. The optimized $Li_{13}Si_4$-010 surface was then used to perform AIMD simulations interacting with liquid EC at 400 K (Figure 2). The unit cell consisted of a $P1$ triclinic cell with vectors 15.84 × 27.00 × 8.88. Twelve EC molecules were used in this case to represent the EC liquid phase (density = 1.32 g/cm^3). Parameters employed for DFT and AIMD simulations are the same reported in section 2.1.

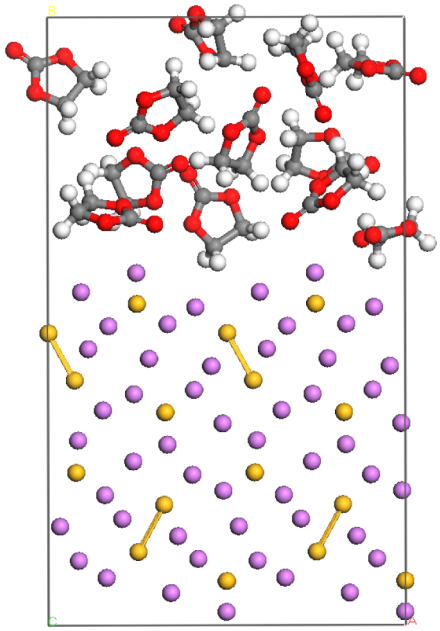

Figure 2. Optimized $Li_{13}Si_4$-010 slab in contact with liquid EC employed for the AIMD simulations at 400 K. Silicon atoms are yellow, lithium atoms are pink, carbon atoms are grey, oxygen atoms are red, and hydrogen atoms are white.

3. RESULTS

3.1. Reduction of Ethylene Carbonate (EC) on Lithium Monosilicide (LiSi). *3.1.1. EC Reduction Mechanism.* Charge analyses allowed the determination of partial atomic charges on the slab models and also on the EC molecules in gas and liquid phase. These charges are reported in Tables 3 and 4. In general,

Table 3. Partial Charges Calculated for the Li and Si Atoms on the LiSi Surfaces[a]

	average charge |e|			
surface	two-fold coordinated Si atoms	three-fold coordinated Si atoms	Li ions	functional group (−H, −O, or −OH)
LiSi-100-H	−0.33	−0.82	0.83	−0.55
LiSi-100-O	0.38	−0.75	0.83	−1.60
LiSi-100-OH	−0.04	−0.79	0.82	−0.94
LiSi-101-H	−0.29	−0.83	0.82	−0.50
LiSi-101-O	0.62	−0.81	0.83	−1.57
LiSi-101-OH	−0.01	−0.82	0.83	−0.85

[a]Charges for the functional groups terminating the two-fold coordinated silicon atoms are also reported.

Table 4. Partial Charges Calculated for the EC Molecule in Gas and in Liquid Phase[a]

	average charge |e|				
EC molecule	O_1	O_2	C_1	C_2	H
gas-phase	−1.10	−1.00	2.09	0.39	0.08
liquid-phase	−1.13	−0.97	1.99	0.31	0.12

[a]See Figure 1 for nomenclature.

Li^+ ions have a positive charge corresponding to +0.82|e|, three-fold coordinated silicon atoms (the 4th coordination is to Li) have a negative charge close to −0.8|e|. Two-fold coordinated silicon atoms (the 3rd coordination is to Li) have a less negative charge that depends on the functional group to which they are bonded, approximately −0.3|e| for silicon atoms bonded to hydrogen, between +0.4|e| and +0.6|e| for those bonded to oxygen, and close to 0|e| for silicon atoms bonded to hydroxyl groups. Hwang et al. showed the relationship between Si−Si coordination and the charge state in bulk and amorphous Li_xSi_y alloys.[43] They calculated a charge of −0.8|e| for three-fold coordinated silicon atoms forming rings in bulk phase LiSi, and +0.84|e| for the Li cations, in very good agreement with our results. Additionally, a decrease in negative charge to approximately −0.73|e| is reported for silicon atoms on slabs as the average coordination of the atoms decreases compared with that in bulk phase. In these surfaces, the net charge of two-fold coordinated silicon atoms is ultimately defined by the functional group interacting with the surface silicon atoms.

Regarding the EC molecule, a significant charge distribution is observed for the molecule in both gas and liquid phases; the largest partial charges are found for the oxygen atoms and the C_1 atom, corresponding to approximately −1.1|e| and +2.0|e|, respectively. Large dipole moments have been previously reported for the EC molecule.[38] The nomenclature used for the EC atoms is defined in Figure 1.

Specific reduction products obtained for all of the different LiSi surfaces after 8 ps of AIMD simulations at 400 K are reported in Table 5. The path followed by all the EC molecules

Table 5. Reduction Products Observed on LiSi Surfaces after 8 ps of AIMD Simulations at 400 K[a]

surface	run	EC ring-opened ($OC_2H_4OCO^{2-}$)	C_2H_4 + CO_3^{2-}
LiSi-100-H	1	0	0
	2	1	0
LiSi-100-O	1	0	0
	2	1	0
LiSi-100-OH	1	0	0
	2	0	0
LiSi-101-H	1	3	1
	2	2	0
LiSi-101-O	1	3	0
	2	1	0
LiSi-101-OH	1	2	0
	2	4	0

[a]Runs 1 and 2 refer to two different initial configurations used in every surface to account for randomness of the EC liquid phase. No adsorption or reduction of the EC molecule was observed in any case when the molecule was in gas phase.

reduced on LiSi surfaces was carefully analyzed to determine their adsorption mechanism. Differences in reactivity between the various LiSi surfaces are discussed in the following section.

The mechanism by which EC molecules adsorb on LiSi surfaces seems to be independent of both the crystallographic plane and the functional group terminating the two-coordinated silicon atoms. In all the six different surfaces employed (LiSi-100-H, LiSi-100-O, LiSi-100-OH, LiSi-101-H, LiSi-101-O, and LiSi-101-OH), the process starts with electrostatic interactions between the negatively charged O_1 of the molecules (see Figure 1 and Table 4) and Li^+ ions, which allows some of the molecules to get closer to the surface. Usually, O_1−Li^+ distances are around 2 Å, and as a result, C_1−Si distances for these molecules oscillate between 3.5 and 4.5 Å. The C_1−Si distance is very important because the transference of charge responsible for the adsorption of the EC molecule takes place between a silicon atom on the surface and the C_1 atom of EC. As has been reported earlier, the LUMO of solution phase EC localizes around the C_1 atom, and the addition of electrons to the LUMO results in C_1−O_1 or C_1−O_2 bond stretching.[27]

Figure 3 shows the fluctuation of C_1−Si distances for 6 of the 13 EC molecules interacting with a LiSi-101-H surface. It is concluded that 4 Å can be considered the critical distance for adsorption, since EC molecules with C_1−Si interactions oscillating around this value *may* adsorb on the surface. However, adsorption will take place only if the C_1 atom is able to get closer to the Si-atom. The ability of the molecule to come closer to the surface appears to be a result of the interaction with other surrounding molecules, given that no adsorption is observed in any case when the EC molecule is in gas phase. Explicit treatment of solvent EC molecules, which display large dipole moments, has been previously found to facilitate the dissociation of molecules compared with gas-phase reaction.[25−27,38] Once the C_1−Si distance is smaller than 3.5 Å, adsorption of the molecule takes place along with a significant

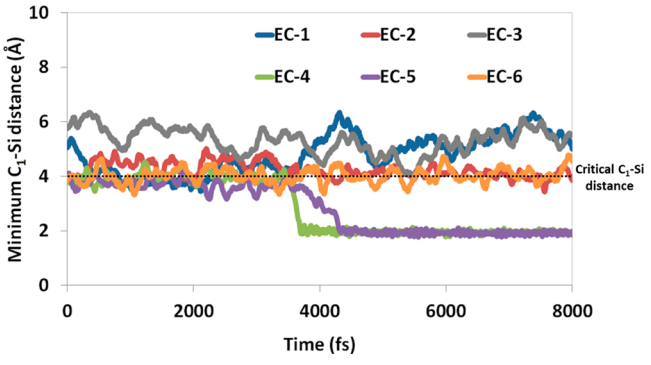

Figure 3. Fluctuation of the C_1−Si distance during 8 ps of AIMD simulations for 6 of the 13 EC molecules modeling the liquid phase in contact with a LiSi-101-H surface; 4 Å can be considered the critical distance for adsorption, since EC molecules with C_1−Si interactions oscillating around this value *may* adsorb on the surface. EC molecules 4 and 5 get adsorbed on the surface after about 4 ps of simulation.

transference of charge from the surface to the molecule. Figure 4 shows the adsorption mechanism for an EC molecule on the LiSi-101-H surface and the charge displayed by the molecule at each step.

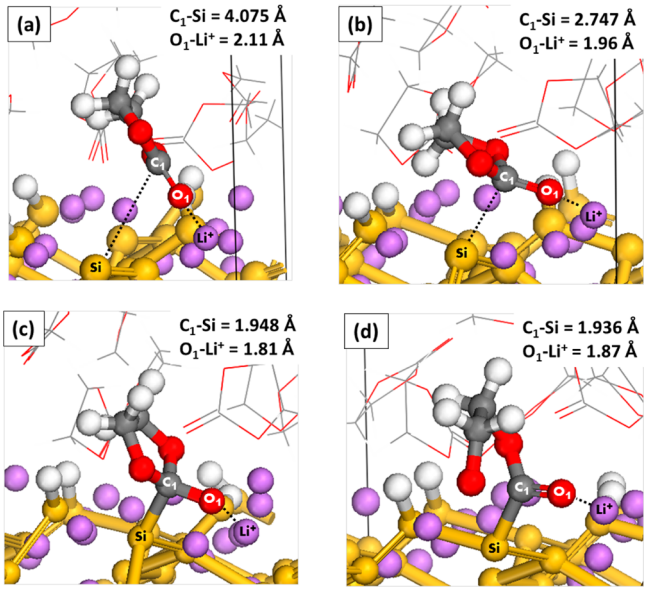

Figure 4. Example of the adsorption mechanism followed by EC molecules on LiSi surfaces. Panels a−d show an EC molecule adsorbing on the LiSi-101-H surface. The adsorption starts with O_1−Li^+ interactions (panel a), once the molecule gets closer to the surface (C_1−Si < 3.5 Å, panel b) adsorption of the molecule takes place (panel c) and a C_1−O_2 bond breaks (panel d). The net charge of the molecule is −0.07|e|, −0.64|e|, −1.46|e|, and −1.66|e| in panels a, b, c, and d respectively.

The net charge of EC molecules as a function of the C_1−Si distance was calculated for several molecules adsorbing on the different LiSi surfaces. It was found that molecules inside the liquid region (*far* from the surface) have net charges practically equal to zero, whereas small negative charges are calculated for molecules closer to the surface. For C_1−Si distances slightly below 4.5 Å, the molecules display an average charge of −0.1|e|, this charge remains practically constant up to a C_1−Si distance of 3.5 Å. For shorter distances, the negative charge monotonically increases as the C_1−Si distance decreases, until adsorption takes place (C_1−Si ≈ 1.9 Å). Figure 5 shows the calculated

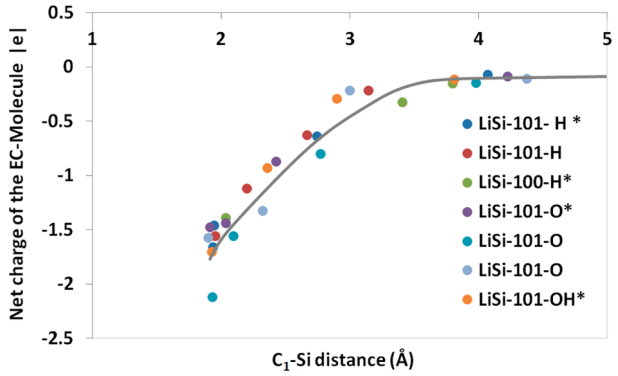

Figure 5. Net charges of EC molecules on different LiSi surfaces as a function of their distance to the surface (C_1−Si distance). The asterisks denote cases in which the molecule is adsorbed on two-fold coordinated silicon atoms. Other cases refer to molecules adsorbing on three-fold coordinated silicon. In both cases, the Si atom is also coordinated to Li.

charge of EC molecules adsorbing on the LiSi-100 and LiSi-101 surfaces. From the figure it is evident that there are no significant differences in the electrostatic interaction of LiSi surfaces with the EC molecules and that the charge transferred is mostly dependent on the C_1−Si distance. Moreover, charge transfer is not significantly influenced by the functional group capping the silicon atoms or even by the nature of the silicon atom where the molecule is being adsorbed (two- or three-fold coordinated).

The charge analysis also reveals that the adsorption of molecules takes place through a two-electron mechanism, similar to the one reported for the dissociation of EC molecules on graphitic anodes and on lithium metal surfaces.[25−27,38,44] Most of the molecules adsorbed on the LiSi surfaces have net negative charges close to −2|e| and a broken C_1−O_2 bond, yielding the $O(C_2H_4)OCO^{2-}$ species (see Table 5 and Figure 4d). The C_1−O_2 bond has been reported to be the weakest in EC^-−Li^+ complexes found in liquid-phase EC,[44] and it was observed to break irreversibly when EC molecules were adsorbed on lithium−metal anodes.[27] Reaction 2 describes the reduction pathway followed by EC molecules adsorbing on lithium monosilicide surfaces (same pathway shown in Figure 4).

$$EC_{(ads)} + 2e^- \rightarrow O(C_2H_4)OCO^{2-}{}_{(ads)} \quad (2)$$

Interestingly, reaction 2 was not the only reduction mechanism observed on LiSi surfaces. In one of the cases, an EC molecule further decomposes into a C_2H_4 + CO_3^{2-} pair (see Table 5). Contrary to the mechanism in reaction 2, EC reduction takes place in the liquid phase. This latter case was further analyzed, and charges were calculated for the different steps in the decomposition process (Figure 6). Initially, a single electron is transferred from the surface to a lithium-coordinated EC molecule, causing a C_2−O_2 bond to break. Subsequently, a second electron is transferred to the EC^- anion, triggering the breaking of a second C_2−O_2 bond and generating the C_2H_4 + CO_3^{2-} pair. This second reduction mechanism, described by reactions 3 and 4, was first introduced in an earlier analysis of EC reduction,[29] and it has recently suggested to be favored when electron tunneling rates from the electrode to the

dx.doi.org/10.1021/am404365r | ACS Appl. Mater. Interfaces 2013, 5, 13457−13465

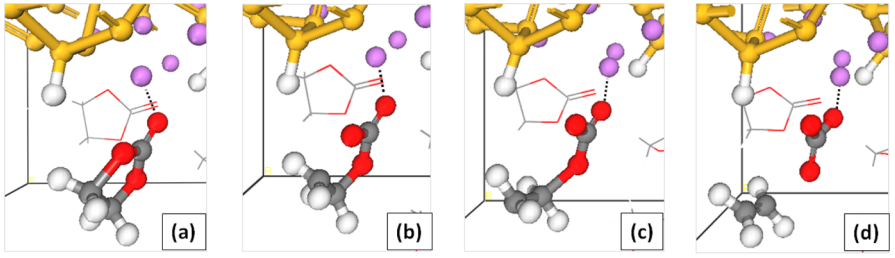

Figure 6. Decomposition of an EC molecule in the liquid phase, following reactions 3 and 4. Initially, a single electron is transferred from the surface to the lithium-coordinated EC molecule (panel a), causing a C_2-O_2 bond to break (panel b). Subsequently, a second electron is transferred to the EC^- radical anion (panel c), triggering the breaking of a second C_2-O_2 bond and generating the C_2H_4 + CO_3^{2-} pair (panel d). The net charges of the EC molecule or the CO_3^{2-}/C_2H_4 products are shown at the bottom of each panel.

electrolyte are slow.[25] However, this example illustrates that this sequential two-electron transfer may also happen (although much less frequently) when the molecule is in direct contact with the electrode surface at low stages of lithiation. Reaction products in reactions 2−4 have been commonly observed during decomposition of EC molecules in solution phase and also for simulations using explicit EC/electrode interfaces.[25−27,38,44]

$$EC + 1e^- \rightarrow EC^- \quad (3)$$

$$EC^- + 1e^- \rightarrow CO_3^{2-} + C_2H_4 \quad (4)$$

3.1.2. Relative Reactivity of LiSi-100 and LiSi-101 Surfaces. Looking at the reduction products in Table 5, it is evident that the LiSi-101 surface is more reactive than the (100) towards EC reduction, with the 100-OH surface being the least reactive. To understand the reason for reactivity differences among the surfaces we refer to the EC adsorption mechanism. The first step required for the adsorption of an EC molecule is the O_1-Li^+ interaction. The more EC molecules are interacting with the surface the larger the number of $Si-C_1$ interactions around 4 Å (the critical distance for adsorption) and, therefore, the larger the probability of molecules getting adsorbed. In the LiSi-101 case, the Li^+ ions are *free* enough to interact with the O_1 atoms of EC molecules. The average nearest-neighbor (NN) distances for Li^+ ions are 2.50, 2.27, and 2.39 Å for the LiSi-101-H, LiSi-101-O, and LiSi-101-OH surfaces, respectively. The negative charge born by the oxygen and hydroxyl species plays a role attracting Li^+ ions and causing smaller NN distances than in the case of the surface with hydrogen terminations. However, calculated NN distances are still large enough to allow easy O_1-Li^+ interactions (as it will be shown in Figure 8). In the other hand, the average NN distances for Li^+ ions in the LiSi-100 surfaces are much shorter. They correspond to 2.20, 2.05, and 2.00 Å for the LiSi-100-H, LiSi-100-O, and LiSi-100-OH surfaces, respectively. In the LiSi-100-O and LiSi-100-OH cases, the Li^+ ions are so close to the O^{2-} and OH^- species, respectively, that the interaction between negatively charged O_1 atoms and Li^+ ions becomes difficult. Consequently, not enough EC molecules are able to come closer to the LiSi surface, resulting in poorer reactivity of these systems.

This effect is more clearly observed in Figures 7 and 8, where the fraction of EC molecules with $Si-C_1$ interactions below 4 Å is plotted against time. Figure 7 follows the trend expected from the calculated NN distances of Li^+ ions, the LiSi-100-H presents a higher number of $Si-C_1$ interactions than the LiSi-100-O and the LiSi-100−OH surfaces. Averages calculated over the 8 ps of AIMD simulation, for two different runs in every surface, are 0.015, 0.085, and 0.145 $Si-C_1$ interactions per silicon atom on the surface per femtosecond, for the LiSi-100-OH, LiSi-100-O, and LiSi-100-H, respectively. These numbers have a direct relation with the reactivity displayed by the different surfaces (number of reduction products observed for each case, Table 5). Furthermore, Figure 8 does not show significant differences in the number of $Si-C_1$ interactions on

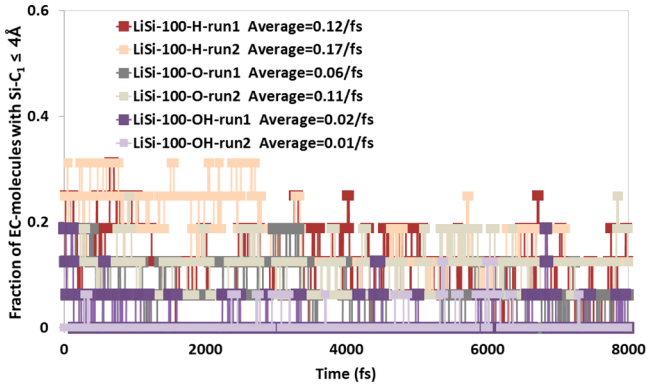

Figure 7. Fraction of EC molecules with $Si-C_1$ interactions below 4 Å for the different LiSi-100 surfaces studied as a function of time. Runs 1 and 2 refer to two different initial configurations used in every surface to account for randomness of the EC liquid phase. Averages calculated over the 8 ps of AIMD simulations are also shown.

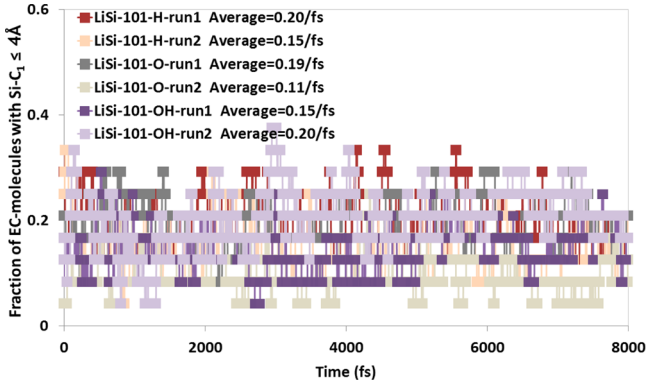

Figure 8. Fraction of EC molecules with $Si-C_1$ interactions below 4 Å for the different LiSi-101 surfaces studied, as a function of time. Runs 1 and 2 refer to two different initial configurations used in every surface to account for randomness of the EC liquid phase. Averages calculated over the 8 ps of AIMD simulations are also shown.

the different LiSi-101 surfaces. Calculated averages are 0.175, 0.145, and 0.175 Si−C_1 interactions per silicon atom on the surface per femtosecond for the LiSi-101−OH, LiSi-101-O, and LiSi-101-H, respectively. It is important to notice that these averages are higher compared with the ones calculated for the LiSi-100 surfaces. This explains the higher reactivity of the LiSi-101 crystallographic plane and also the similar number of reaction products observed on the three functionalized (101) surfaces.

In summary, the reactivity of LiSi surfaces is mainly determined by the ability of EC molecules to interact with Li^+ ions on the surface. The specific crystallographic plane and also different terminations (−H, −O, or −OH) affect Li^+ ion NN distances on the surface, and if these are too short, Li^+−EC interactions are hindered. In the case of LiSi-101 surfaces, Li^+ NN distances are all above 2.27 Å; this distance seems to be long enough to easily allow Li^+−EC interactions since no significant differences are observed in the reactivity of LiSi-101 surfaces towards EC reduction. However, in the case of LiSi-100 surfaces, Li^+ NN distances are much shorter, all of them below 2.20 Å. These short distances result in poorer reactivity towards EC reduction since not enough molecules are able to approach the surface (as shown in Figure 7). This reactivity trend driven by geometrical differences among LiSi surfaces differs from the one found on graphitic anodes.[44] In that case, the reactivity was determined by the electrochemical activity of the functional groups terminating the graphitic surface. Therefore, hydrogen terminations were found to be inactive towards EC reduction, and highly oxidized sites were found to be the most active.

3.2. Reduction of Ethylene Carbonate (EC) on Low-Lithiated $LiSi_4$ and $LiSi_2$ Surfaces. Figure 9a,b shows the optimized unit cells of $LiSi_2$-100-H and $LiSi_4$-100-H surfaces, respectively. A larger deformation of the tetrahedral silicon structure is found for the $LiSi_4$-100-H case due to the lower ionic stability of the silicon rings in this system. Additionally,

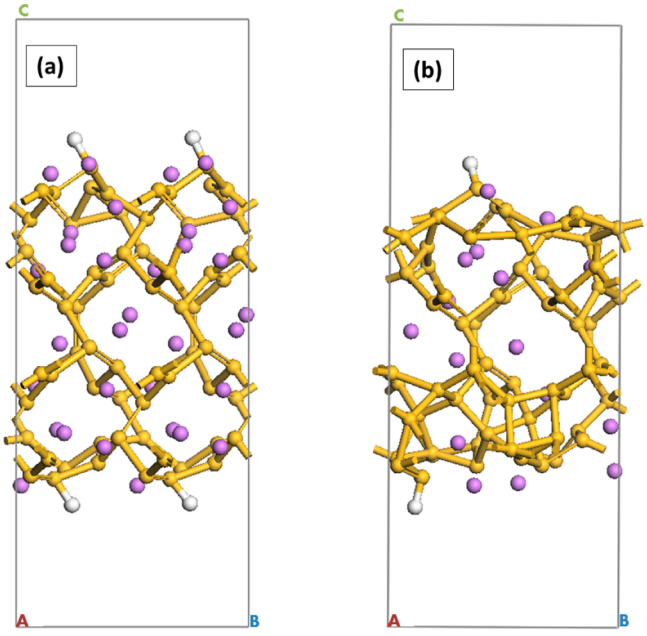

Figure 9. Unit cell of (a) the $LiSi_2$-100-H surface and (b) the $LiSi_4$-100-H surface. Silicon atoms are yellow, lithium atoms are pink, and hydrogen atoms are white.

silicon atoms on the topmost layer of these surfaces undergo larger reconstruction than in the LiSi system, resulting in a smaller number of two-fold coordinated silicon atoms (four in the $LiSi_2$-100-H surface and two in the $LiSi_4$-100-H). Average calculated charges for Li^+ ions correspond to +0.83|e| in both surfaces, whereas calculated charges for silicon are directly related to the content of lithium in the surface, corresponding to −0.41|e| in the $LiSi_2$-100 surface and −0.21|e| in the $LiSi_4$-100. Such relationship is expected from the ionic nature of these crystals, in which the negative charge of silicon anions results from a direct transference of electrons from lithium. Hwang et al. calculated a negative charge of −0.35|e| for three-fold coordinated silicon atoms forming rings in bulk phase $LiSi_{2.5}$ and +0.85|e| for lithium ions,[43] similar to the charges calculated in this work for the $LiSi_2$-100 surface. Investigation of the EC reduction in $LiSi_4$-100-H and $LiSi_2$-100-H surfaces will allow identification of possible differences in the mechanism given by variations in the electrostatic state of silicon at lower lithiation stages.

Only one initial configuration was used in these systems to perform the AIMD simulations; therefore randomness of the liquid phase is not fully taken into account. In consequence, comparisons with the reactivity of LiSi surfaces will not be discussed but rather possible differences in the EC reduction mechanism due to the lower lithiation stage. Adsorption of an EC molecule was observed in the $LiSi_4$-100-H surface after 4 ps of simulation at 400 K, while in the $LiSi_2$-100-H surface it was observed after 16 ps (much longer time compared to those in Figure 3, but better statistics are needed to confirm). The reduction mechanism observed in both surfaces corresponds to that depicted in Figure 4. Charges calculated at different C_1−Si distances during the adsorption are shown in Table 6. When

Table 6. Net Charge of EC Molecules Adsorbing on $LiSi_2$-100-H and on $LiSi_4$-100-H Surfaces as a Function of the C_1−Si Distance

$LiSi_2$-100-H		$LiSi_4$-100-H	
C_1−Si distance (Å)	net charge |e|	C_1−Si distance (Å)	net charge |e|
1.90	−1.56	2.00	−1.43
2.00	−1.49	2.50	−0.92
2.86	−0.57	2.95	−0.57
3.39	−0.17	3.23	−0.14
3.97	−0.09	3.72	−0.11

these data are plotted along with those in Figure 5, no significant differences are observed among the electrostatic interaction of EC molecules with LiSi, $LiSi_2$, or $LiSi_4$ surfaces (Figure 5 including the data for $LiSi_2$ and $LiSi_4$ surfaces can be found as Supporting Information). In all of these cases, the molecule is reduced through the most common two-electron mechanism (reaction 2 described in section 3.1.1). Results presented in this section suggest that EC reduction may be possible from very early lithiation stages of the silicon anode, that is, even before the first stable silicon alloy crystal (LiSi) is formed.

3.3. Reduction of Ethylene Carbonate (EC) on a Highly Lithiated $Li_{13}Si_4$-010 Surface. Charge analysis performed on the $Li_{13}Si_4$-010 surface allowed the determination of partial charges of the different atoms on the slab model (Figure 2). Li^+ ions have a positive charge corresponding to +0.80|e|, isolated silicon atoms have a negative charge corresponding to −3.2|e|, and silicon atoms forming dumbbells have a charge

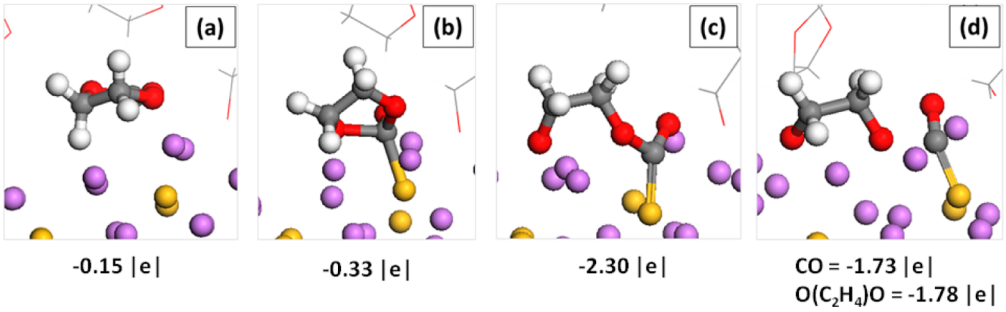

Figure 10. Decomposition of an EC molecule on the $Li_{13}Si_4$-010 surface, following reactions 2 and 5. (a, b) Adsorption of the molecule takes place due to transference of charge between a Si-atom on the surface and the C_1 of the EC molecule; (c) upon transference of two electrons to the adsorbed molecule, one of its C_1-O_2 bonds is broken; (d) after a few more picoseconds of simulation, two more electrons are transferred to the adsorbed EC anion, resulting in the formation of $CO^{2-}{}_{(ads)}$ and $O(C_2H_4)O^{2-}$. The net charges of the EC molecule or the $CO^{2-}/O(C_2H_4)O^{2-}$ products are shown at the bottom of each panel.

corresponding to −2.0|e|. These values are in agreement with those calculated by Chevrier et al, which found four total electrons shared by silicon atoms forming dumbbells and a charge of −4|e| for isolated silicon atoms.[22] The higher number of valence electrons available in this system compared with those in $LiSi_4$, $LiSi_2$, and LiSi may allow faster electron transfer regimes.

After 8 ps of AIMD simulations, two of the EC molecules in the liquid phase were found reduced through direct adsorption on silicon atoms (Figure 10). The first step takes place through the two-electron mechanism described by reaction 2, with transference of charge between a Si-atom on the surface and the C_1 atom in the EC molecule. However, upon adsorption of the EC molecule on the surface (Figure 10b) and breaking of the first C_1-O_2 bond (Fig. 10c), two more electrons are transferred to the adsorbed anion, triggering the breaking of a second C_1-O_2 bond and generating as reduction products $CO^{2-}{}_{(ads)}$ and $O(C_2H_4)O^{2-}$ as described in reaction 5 and Figure 10d.

$$O(C_2H_4)OCO^{2-}{}_{(ads)} + 2e^- \rightarrow O(C_2H_4)O^{2-} + CO^{2-}{}_{(ads)} \quad (5)$$

Three other EC molecules were reduced in this system. However, they were not adsorbed on the surface, and the reduction took place through direct transference of electrons from the $Li_{13}Si_4$ slab to nearby EC molecules in the liquid phase. In contrast to the sequential transference of electrons from the LiSi slab to EC molecules in the liquid phase (reactions 2 and 3), in this case the surface releases two electrons simultaneously, causing the breaking of a C_1-O_2 bond of the molecule, instead of two C_2-O_2 bonds. As a result, some $O(C_2H_4)OCO^{2-}$ anions are found in the liquid phase of EC in contact with the $Li_{13}Si_4$ surface.

No CO_3^{2-}/C_2H_4 pairs were observed in this simulation, but it is also possible for EC molecules in contact with $Li_{13}Si_4$ surfaces to dissociate following this mechanism (reactions 2 and 3). Leung and coworkers found EC molecules dissociating into CO_3^{2-}/C_2H_4 pairs in a simulation of FEC and EC molecules in contact with the $Li_{13}Si_4$ surface.[28] Reduction products in reaction 5 and $O(C_2H_4)OCO^{2-}$ anions in the liquid phase have also been previously found by these researchers after reduction of EC on graphitic anodes, as well as on $Li_{13}Si_4$ surfaces in the presence of fluoroethylene carbonate.[28,44]

Comparison of results in this section with those in sections 3.1.1 and 3.2 shows a dependence of the EC reduction mechanism on the lithiation state of the silicon anode. At early lithiation stages ($LiSi_4$, $LiSi_2$, and LiSi), reduction of EC molecules takes place through two different two-electron mechanisms, described by reactions 2, and 3 and 4 respectively. Reaction 2 corresponds to an adsorbed EC^{2-} anion, and reactions 3 and 4 describe two subsequent one-electron transfers to the same EC molecule in liquid phase, generating a CO_3^{2-}/C_2H_4 pair. In the other hand, reduction of EC molecules on strongly lithiated silicon anodes ($Li_{13}Si_4$) takes place through a four-electron mechanism described by reactions 2 and 5, generating an adsorbed CO^{2-} and the $O(C_2H_4)O^{2-}$ fragment in liquid phase. Transference of two electrons to EC molecules in liquid phase is also observed. However, as explained above, the two electrons are transferred to the EC molecule simultaneously, resulting in the breaking of a C_1-O_2 bond of the EC^{2-} anion. In some cases, EC may also be reduced in the presence of the strongly lithiated surface through reactions 3 and 4, generating a CO_3^{2-}/C_2H_4 pair. These results have important implications for the formation of the SEI layer because different adsorbed species and charged fragments in the liquid phase may participate in various subsequent reactions with molecules or fragments present in the solvent and electrolyte. This may result in SEI layers with different composition and physical properties at different lithiation stages of the anode.

4. CONCLUSIONS

The reduction of ethylene carbonate (EC) on lithiated silicon surfaces was investigated using AIMD based simulations. At an intermediate stage of lithiation, EC reduces on LiSi surfaces following two different two-electron mechanisms, which are independent of specific surface features (e.g., crystallographic plane or functional group terminating silicon atoms on the surface). In the most common reduction path, the molecule is adsorbed on the surface, and two-electron transfer from the surface to an adsorbed molecule results in the breaking of a C_1-O_2 bond, yielding the $O(C_2H_4)OCO^{2-}$ adsorbed species. In the second (less common) reduction path, a sequential two-electron transfer takes place in the liquid phase. First, a lithium-coordinated EC molecule receives an electron from the surface; subsequently, the EC^- anion with a broken C_2-O_2 bond receives another electron, which induces a second C_2-O_2 bond breaking and yields a $C_2H_4 + CO_3^{2-}$ pair. When comparing these mechanisms with the ones observed for molecules reducing on lower-lithiated $LiSi_2$ and $LiSi_4$ surfaces, we found that EC reduction follows the most common reduction path. These results suggest that decomposition of EC may start at

very early stages of lithiation (even before LiSi is observed, voltages >0.39 V vs Li^+/Li metal).

Strongly lithiated $Li_{13}Si_4$ surfaces are found to be highly reactive. Reduction of adsorbed EC molecules takes place through a four-electron mechanism yielding as reduction products CO^{2-} and $O(C_2H_4)O^{2-}$. Direct transfer of two electrons to EC molecules in liquid phase is also possible, resulting in the presence of $O(C_2H_4)OCO^{2-}$ anions in the liquid phase. Thus, reduction mechanisms of EC on lithiated silicon anodes are clearly dependent on the lithiation stage of the anode. The presence of various charged fragments (anions and radical anion species), both adsorbed and in liquid phase, is expected. These fragments may participate in subsequent attacks to intact molecules in the electrolyte resulting in SEI layers with physical, chemical, and transport properties depending on the lithiation stage of the silicon anode.

Differences in reactivity among the six LiSi surfaces studied (LiSi-100-H, LiSi-100-O, LiSi-100-OH, LiSi-101-H, LiSi-101-O, and LiSi-101-OH) were also analyzed. Reactivity was found to depend on the ability of EC molecules to interact with Li^+ ions on the surfaces, which is determined by Li^+ NN distances. Short distances result in poorer reactivity towards EC reduction since not enough molecules are able to approach the surface. This reactivity trend driven by geometrical differences among LiSi surfaces differs from the one found on graphitic anodes where reactivity is determined by the electrochemical activity of the functional groups terminating the surface.

■ ASSOCIATED CONTENT

Supporting Information

Figure S1 reproduces Figure 5 including charge data for the $LiSi_2$ and $LiSi_4$ systems. This material is available free of charge via the Internet at http://pubs.acs.org.

■ AUTHOR INFORMATION

Corresponding Author

*E-mail: balbuena@tamu.edu.

Notes

The authors declare no competing financial interest.

■ ACKNOWLEDGMENTS

J.M.M. and P.B.B. were supported by the Assistant Secretary for Energy Efficiency and Renewable Energy, Office of Vehicle Technologies of the U.S. Department of Energy, under Contract No. DE-AC02-05CH11231, Subcontract No. 7060634, under the Batteries for Advanced Transportation Technologies (BATT) Program. Sandia National Laboratories is a multiprogram laboratory managed and operated by Sandia Corporation, a wholly owned subsidiary of Lockheed Martin Corporation, for the U.S. Department of Energy National Nuclear Security Administration under Contract DE-AC04-94AL85000. Computational resources from Texas A&M Supercomputing Center, Brazos Supercomputing Cluster at Texas A&M University, and from Texas Advanced Computing Center at UT Austin are gratefully acknowledged.

■ REFERENCES

(1) Armand, M.; Tarascon, J. M. *Nature* **2008**, *451*, 652.
(2) Choi, N.-S.; Chen, Z.; Freunberger, S. A.; Ji, X.; Sun, Y.-K.; Amine, K.; Yushin, G.; Nazar, L. F.; Cho, J.; Bruce, P. G. *Angew. Chem., Int. Ed.* **2012**, *51*, 9994.
(3) Goodenough, J. B.; Kim, Y. *Chem. Mater.* **2009**, *22*, 587.
(4) Zhang, W.-J. *J. Power Sources* **2011**, *196*, 13.
(5) Raimann, P. R.; Hochgatterer, N. S.; Korepp, C.; Möller, K. C.; Winter, M.; Schröttner, H.; Hofer, F.; Besenhard, J. O. *Ionics* **2006**, *12*, 253.
(6) Hatchard, T. D.; Dahn, J. R. *J. Electrochem. Soc.* **2004**, *151*, A838.
(7) Zhang, X.-W.; Patil, P. K.; Wang, C.; Appleby, A. J.; Little, F. E.; Cocke, D. L. *J. Power Sources* **2004**, *125*, 206.
(8) *Lithium-Ion Batteries: Solid Electrolyte Interphase*; Balbuena, P. B., Wang, Y. X., Eds.; Imperial College Press: London, 2004.
(9) Xu, K. *Chem. Rev.* **2004**, *104*, 4303.
(10) Nie, M. Y.; Abraham, D. P.; Chen, Y. J.; Bose, A.; Lucht, B. L. *J. Phys. Chem. C* **2013**, *117*, 13403.
(11) Etacheri, V.; Haik, O.; Goffer, Y.; Roberts, G. A.; Stefan, I. C.; Fasching, R.; Aurbach, D. *Langmuir* **2012**, *28*, 965.
(12) Verma, P.; Maire, P.; Novák, P. *Electrochim. Acta* **2010**, *55*, 6332.
(13) Wu, H.; Chan, G.; Choi, J. W.; Ryu, I.; Yao, Y.; McDowell, M. T.; Lee, S. W.; Jackson, A.; Yang, Y.; Hu, L.; Cui, Y. *Nat. Nanotechnol.* **2012**, *7*, 310.
(14) Xianhua, H.; Shejun, H.; Qiang, R.; Zhiwen, Z. *Rare Met. Mater. Eng.* **2010**, *39*, 2079.
(15) Hautier, G.; Jain, A.; Ong, S. P.; Kang, B.; Moore, C.; Doe, R.; Ceder, G. *Chem. Mater.* **2011**, *23*, 3495.
(16) Jain, A.; Hautier, G.; Moore, C. J.; Ping Ong, S.; Fischer, C. C.; Mueller, T.; Persson, K. A.; Ceder, G. *Comput. Mater. Sci.* **2011**, *50*, 2295.
(17) Wang, Y.; Nakamura, S.; Tasaki, K.; Balbuena, P. B. *J. Am. Chem. Soc.* **2002**, *124*, 4408.
(18) Wang, Y. X.; Balbuena, P. B. *Int. J. Quantum Chem.* **2005**, *102*, 724.
(19) Wang, Y.; Balbuena, P. B. *J. Phys. Chem. B* **2002**, *106*, 4486.
(20) Evers, J.; Oehlinger, G.; Sextl, G. *Angew. Chem., Int. Ed.* **1993**, *32*, 1442.
(21) Stearns, L. A.; Gryko, J.; Diefenbacher, J.; Ramachandran, G. K.; McMillan, P. F. *J. Solid State Chem.* **2003**, *173*, 251.
(22) Chevrier, V. L.; Zwanziger, J. W.; Dahn, J. R. *J. Alloys Compd.* **2010**, *496*, 25.
(23) Kubota, Y.; Escaño, M. C. S.; Nakanishi, H.; Kasai, H. *J. Alloys Compd.* **2008**, *458*, 151.
(24) Sholl, D. S.; Steckel, J. A. *Density Functional Theory: A Practical Introduction*; John Wiley & Sons, Inc.: Hoboken, NJ, 2009; p 83.
(25) Leung, K. *Chem. Phys. Lett.* **2013**, *568*−*569*, 1.
(26) Leung, K. *J. Phys. Chem. C* **2013**, *117*, 1539.
(27) Yu, J.; Balbuena, P. B.; Budzien, J.; Leung, K. *J. Electrochem. Soc.* **2011**, *158*, A400.
(28) Leung, K.; Rempe, S. B.; Foster, M. E.; Ma, Y.; Martinez de la Hoz, J.; Sai, N.; Balbuena, P. *J. Electrochem. Soc.* **2013**, Submitted for publication.
(29) Kresse, G.; Furthmüller, J. *Phys. Rev. B* **1996**, *54*, 11169.
(30) Kresse, G.; Furthmuller, J. *Comput. Mater. Sci.* **1996**, *6*, 15.
(31) Kresse, G.; Hafner, J. *Phys. Rev. B* **1993**, *48*, 13115.
(32) Kresse, G.; Hafner, J. *Phys. Rev. B* **1993**, *47*, 558.
(33) Kresse, G.; Hafner, J. *Phys. Rev. B* **1994**, *49*, 14251.
(34) Perdew, J. P.; Burke, K.; Ernzerhof, M. *Phys. Rev. Lett.* **1996**, *77*, 3865.
(35) Blöchl, P. E. *Phys. Rev. B* **1994**, *50*, 17953.
(36) Kresse, G.; Joubert, D. *Phys. Rev. B* **1999**, *59*, 1758.
(37) Monkhorst, H. J.; Pack, J. D. *Phys. Rev. B* **1976**, *13*, 5188.
(38) Wang, Y.; Nakamura, S.; Ue, M.; Balbuena, P. B. *J. Am. Chem. Soc.* **2001**, *123*, 11708.
(39) *DISCOVER*, Accelrys Software Inc, 2010.
(40) Song, C.; Wu, W.; Al-Ostaz, A. In *Proceedings GeoCongress 2008*; Reddy, K. R., Khire, M. V., Alshawabkeh, A. N., Eds.; American Society of Civil Engineers: Reston, VA, 2008, p 1012.
(41) Henkelman, G.; Arnaldsson, A.; Jónsson, H. *Comput. Mater. Sci.* **2006**, *36*, 354.
(42) Sanville, E.; Kenny, S. D.; Smith, R.; Henkelman, G. *J. Comput. Chem.* **2007**, *28*, 899.
(43) Chou, C.-Y.; Hwang, G. S. *Surf. Sci.* **2013**, *612*, 16.
(44) Leung, K.; Budzien, J. L. *Phys. Chem. Chem. Phys.* **2010**, *12*, 6583.